Journal of Zhejiang University-SCIENCE A (Applied Physics & Engineering)
ISSN 1673-565X (Print); ISSN 1862-1775 (Online)
www.jzus.zju.edu.cn; www.springerlink.com
E-mail: jzus@zju.edu.cn

Parameters optimization of a parallel-flow heat exchanger with a new type of anti-vibration baffle and coiled wire using Taguchi method*

Chu-lin YU†[1,2], Zhi-wen REN[2], Min ZENG[2], Min-dong JI[1]

[1]*Clean Combustion and Flue Gas Purification Key Laboratory of Sichuan Province, Dongfang Boiler Group Co., Ltd., Chengdu 611731, China*

[2]*MOE Key Laboratory of Thermo-Fluid Science and Engineering, Xi'an Jiaotong University, Xi'an 710049, China*

†E-mail: yuchulin_007@163.com

Received July 23, 2017; Revision accepted Jan. 29, 2018; Crosschecked Aug. 27, 2018

Abstract: This study presents the thermal-hydraulic optimization of the design parameters of a parallel-flow shell-and-tube heat exchanger with a new type of anti-vibration hexagon clamping baffle and equilateral triangle cross-sectioned coiled wire. A periodic flow unit duct with non-staggered tube layout is adopted as the numerical analysis model by Fluent. The Taguchi method is used to explore the influence of five geometric parameters including baffle distance (A), baffle width (B), coil diameter (C), coil pitch (D), and the side length of the equilateral triangle (E). An L18 (3^5) orthogonal array is chosen to carry out the numerical simulation. The comprehensive thermal-hydraulic performance evaluation criterion (PEC) is set as the optimization goal. The results show that the order of the factor effectiveness for the Nusselt number is E>C>A>D>B, for the flow friction is C>E>A>B>D and for the PEC is C>E>A>B>D. This means that the coil pitch has a great influence while the baffle width and the coil diameter have a trifling effect. Finally, the optimal factor combination for PEC is obtained. The PEC of the optimal combination is 0.19%–1.92% higher than the model with better comprehensive performance among 18 cases for Reynolds number in the range from 14465 to 32547.

Key words: Optimization; Parallel-flow; Anti-vibration; Hexagon clamping baffle; Coiled wire; Taguchi method
https://doi.org/10.1631/jzus.A1700385 **CLC number:** TK124

1 Introduction

Shell-and-tube heat exchangers (STHXs) are applied in a variety of industrial fields because of their low cost and adaptability (Huang et al., 2008). In STHXs, the shape and arrangement of the baffles are of essential importance for thermal-hydraulic performance (El Maakoul et al., 2016). According to the flow direction of shell side, the STHXs can be divided into three groups: transverse flow, helical flow, and longitudinal flow (Wang et al., 2011).

STHXs with segmental baffles (SB-STHXs) are typical transverse flow heat exchangers. They have many advantages, such as easy manufacturing and low cost. However, they also have many disadvantages, such as large pressure drop, low heat transfer efficiency, and harmful vibration (Zhang et al., 2013).

STHXs with helical baffles (HB-STHXs) have some advantages such as high heat transfer efficiency and low flow resistance (Chen et al., 2013). Numerical and experimental investigations have been conducted to explore the heat transfer and pressure drop in many novel HB-STHXs (Master et al., 2003; Wang et al., 2009; Zhang et al., 2009). However, the use of

* Project supported by the National Science and Technology Major Project of the Ministry of Science and Technology of China (No. 2010ZX06004-013) and the Specialized Research Fund of the Postdoctoral Program of the Dongfang Boiler Group Co., Ltd., China
ORCID: Chu-lin YU, https://orcid.org/0000-0001-8459-5520

HB-STHXs is still limited as the helical baffles are difficult to manufacture.

STHXs with longitudinal baffles (LB-STHXs) have been widely used in various industries (Wang et al., 2007). LB-STHXs can enhance heat transfer, reduce pressure loss, eliminate stagnant recirculation zones, strengthen fluid turbulence, and avoid flow-induced tube vibration (Gentry, 1990). For the past decades, although many new longitudinal baffles, such as ring baffle (Deng and Deng, 1998), large and small hole baffles (Sheng et al., 2012), plate baffle (Yang and Liu, 2015), and trefoil-hole baffle (You et al., 2015) have been proposed, the round rod baffle (RRB) is still one of the main design choices because of its satisfactory overall thermal-hydraulic performance and low cost (Dong et al., 2008).

Not surprisingly, the STHXs with round rod baffles (RRB-STHXs) also have some limitations and drawbacks: (1) the baffle distance, usually between 110 and 150 mm, must be small in order to enhance the heat transfer rate; (2) the heat transfer rate may be very low when the mass flow on the shell side is small; (3) the tube may be worn to leakage by a point contact between the tube and the RRB (Hutagalung, 2014). In order to solve the problems of RRB-STHX mentioned above, a type of curve-rod baffle (CRB) with good vibration-preventing performance has been proposed (Yan et al., 2004; Li et al., 2005). It was found that this CRB can not only support the tube bundle effectively, but can also enhance the heat transfer in case of low Reynolds number. Inspired by the fixed strip of economizer used in the boiler, a new type of anti-vibration baffle, the hexagon clamping baffle (HCB) is proposed in this paper. A picture of a typical tube bundle in a non-staggered alignment supported by the HCB is shown in Fig. 1. The advantages of this structure are as follows: (1) the abrasion between the tube and the HCB can be significantly eased, as the contact area between the tube and the HCB is larger compared with that in the RRB-STHX; (2) the baffle distance can be increased to reduce the excessive use of HCB because the rigidity of the HCB is much stronger than that of the RRB; (3) the HCB can be used with some other parts such as twisted tape, wire coil to further enhance the heat transfer rate.

Previous studies have explored the heat transfer and pressure drop in tubes with different coiled wire

Fig. 1 Picture of tube bundle supported by the HCB

inserts. The thermal-hydraulic performance between twisted tape and coiled wire inserts for both laminar and turbulent flow regimes has been compared (Wang and Sundén, 2002). It was found that the coiled wire inserts provided a better overall enhancement than the twisted tape inserts in a turbulent flow regime. The thermal performance of a tube with square cross-sectioned coiled wire was experimentally studied and compared with that obtained from that using circular cross-sectioned coiled wire (Promvonge, 2008). It was found that the Nusselt number increased with the reduction of pitch for both circular and square wire coils and the coiled square wire gave a higher heat transfer rate than the circular one under the same conditions. Considering that attaching the inserts to the tube wall may cause contamination over time and result in additional resistance to heat transfer, the thermal-hydraulic performance of a circular tube with coiled wire inserts installed with a small separation from the inner wall of the tube was experimentally studied (Keklikcioglu and Ozceyhan, 2016). Results showed that the maximum thermal performance was around 1.82 at a Reynolds number of 3429. The heat transfer and pressure drop of a tube with equilateral triangle cross-sectioned coiled wire inserted in the turbulent flow regime was experimentally investigated (Gunes et al., 2011). The effects on heat transfer of three different pitch ratios and two different ratios of triangle length side to tube diameter in the range of Reynolds number from 3500 to 27000 were discussed. It was found that the coiled wire inserts led to a considerable increase in heat transfer and pressure drop compared with the smooth tube. Computations were performed for the forced convective heat transfer of an Al_2O_3–water nanofluid over an equilateral triangular obstacle with three different orientations (side, vortex, and diagonal facing flows). Results showed that the heat enhancement of the vortex-facing flow orientation was better than that of the side-facing flow orientation when the nanoparticles were not available (Bovand et al., 2015). The entropy

generation of a circular tube inserted with coiled wire inserts was experimentally explored. The wire inserts were manufactured with an equilateral triangular cross-section and were coiled so that a vortex-facing flow orientation was adopted. Results showed that the entropy generation number increased with increasing Reynolds number and decreased with increasing pitch ratio (Keklikcioglu and Ozceyhan, 2017).

The applications of classical design methods cannot be sufficiently efficient under industrial conditions. It is not practical to conduct a great number of experiments to optimize the objective because of the very significant time and cost involved in so doing. The Taguchi method was developed by Genichi Taguchi to improve the quality of manufactured goods (Gunes et al., 2011). It is one of the robust design and optimization methods, based on statistical principles, which can finish the process of optimization at a low cost by combining levels of different factors. In the past few years, various heat exchangers have been studied and optimized using the Taguchi method. For example, the effects of design parameters on heat transfer and flow friction characteristics in a heat exchanger equipped with slit type fins were studied based on it (Yun and Lee, 2000). Parameters optimization of a vortex-generator fin-and-tube heat exchanger was numerically carried out using the Taguchi method (Zeng et al., 2010), and it was also employed to achieve the optimum values of the design parameters for heat transfer and pressure drop in a tube equipped with twisted tape (Bas and Ozceyhan, 2014). The determination of the optimum values of the design parameters in a tube with equilateral triangular cross-sectioned coiled wire inserts was investigated using the method (Gunes et al., 2011). It has also been used to study the influence of seven geometric parameters on thermal-hydraulic performance of H-type finned tube heat exchangers (Wang et al., 2016).

In the cases cited, most studies were focused on the heat enhancement of the tube with different inserted wire coils. However, to the best of the authors' knowledge, there are no reports of the study of the heat transfer enhancement from using a combination of HCB and coiled wire in the shell side of the STHXs. This paper is therefore focused on the optimization of the thermal-hydraulic performance of STHX with the HCB and equilateral triangular cross-sectioned coiled wire (HCBetsw-STHX) using the Taguchi method. A sketch of the manufacturing process of the tube bundle supported by the HCB is shown in Fig. 2. The tube bundle supported by the HCB and wire coils is shown in Fig. 3. The detailed profile of the HCB is shown in Fig. 4. The coiled wire with equilateral triangle cross-section is shown in Fig. 5. It is worth mentioning that the vortex-facing flow layout of the equilateral triangle is adopted in this paper because it is effective on laminar sub-layer disturbance. The influence of five geometric parameters (baffle distance, baffle width, coil diameter, coil pitch, and the side length of the equilateral triangle) on heat transfer and pressure drop is numerically investigated. The optimal design value of each parameter is presented, and confirmation tests are carried out. This study gives a useful insight into the design and optimization of the HCBetsw-STHX.

2 Numerical model

2.1 Physical model

A periodic flow unit duct of a non-staggered tube bundle is taken as the simplified model of the shell side to perform a numerical simulation. To simplify the numerical simulation, the following assumptions are made: the working fluid is water which is continuous, Newtonian, and isotropic; the gravity effect is negligible; the thermal radiation and viscous heating are negligible. The thermal-physical properties of water (density ρ=999.7 kg/m^3, thermal conductivity λ=0.574 W/(m·K), specific heat c_p=4191 J/(kg·K), and μ=0.001306 Pa·s) remain constant during the calculation process.

As can be seen from Fig. 6, the computational domain includes the inlet extended block, heat transfer block, and outlet extended block. The inlet extended block is formed by extending the original heat transfer block by 100 mm at the upstream to ensure inlet uniformity. Similarly, the outlet extended domain is formed by extending the original heat transfer block by 100 mm at the downstream so as to avoid backflow. Fig. 7 illustrates an example of the meshed configuration of RRB-STHX and HCBetsw-STHX. As shown in this figure, the fluid zone close to the baffle and wire is meshed into smaller control volumes in order to find more precise prediction results.

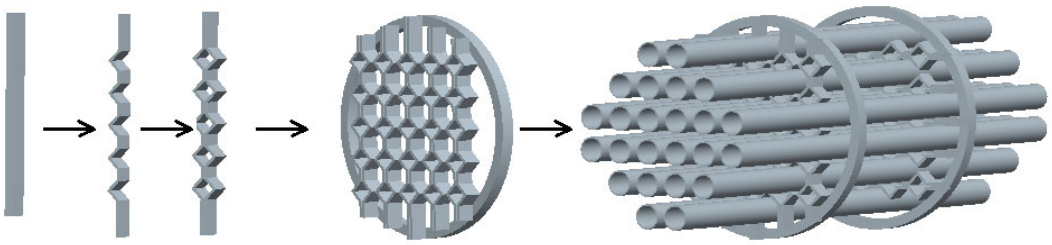

Fig. 2 Sketch of manufacturing process of tube bundle supported by the HCB

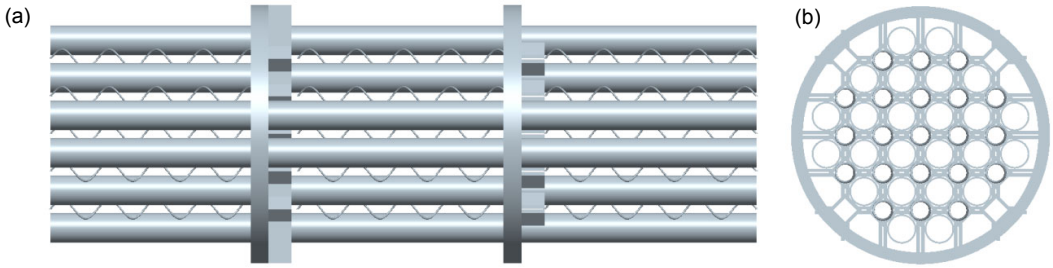

Fig. 3 Sketch of tube bundle with the HCB and wire coils: (a) front view; (b) left view

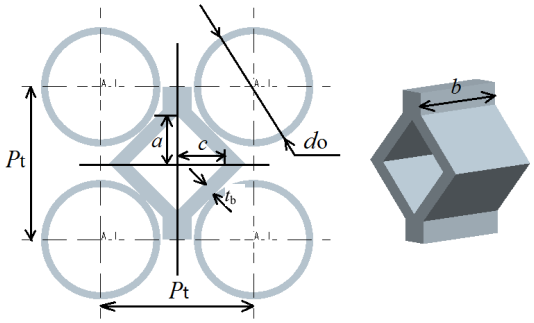

Fig. 4 Detailed profile of the HCB

P_t is the tube pitch (mm); d_o is the outer tube diameter (mm); a and c are side lengths (mm); b is the baffle width (mm); t_b is the baffle thickness (mm)

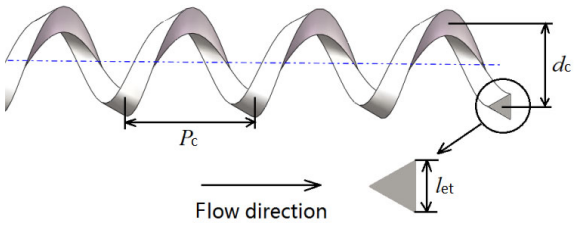

Fig. 5 Sketch of coiled wire with equilateral triangle cross-section

P_c is the coil pitch (mm); d_c is the diameter of circular section (mm); l_{et} is the length of equilateral triangular section (mm)

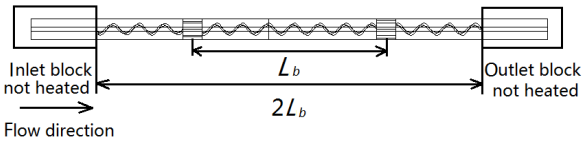

Fig. 6 Schematic diagram of the computational domain of the HCBetsw-STHX

L_b is the baffle distance (mm)

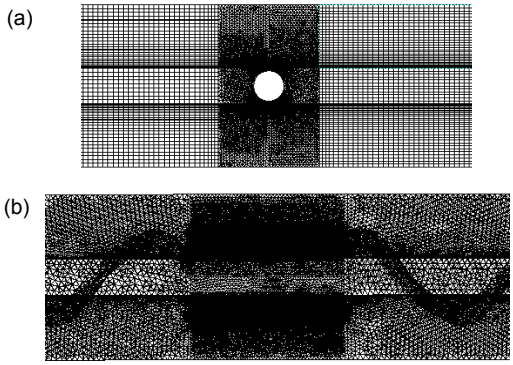

Fig. 7 Flow unit duct mesh of the RRB-STHX (a) and HCBetsw-STHX (b)

2.2 Governing equations

The dimensionless steady equations for continuity, momentum, and energy can be expressed in tensor notation as

$$\nabla(\rho \boldsymbol{V}\phi) = \nabla(\Gamma_\phi \mathrm{grad}\,\phi) + S_\phi, \tag{1}$$

where $\boldsymbol{V}$ is the velocity vector; ϕ stands for the velocity components, temperature, etc.; Γ_ϕ and S_ϕ represent the appropriate diffusion coefficients and the source terms, respectively.

2.3 Numerical method and boundary conditions

The commercial computational fluid dynamics (CFD) software Fluent is adopted for all the numerical simulations. The 3D, double-precision, pressure-based stead state solver is used. The standard wall function method is adopted for the near-wall region. A no-slip boundary condition is imposed at the wire coil walls as well as on the unit duct wall. The surfaces of the baffles are set as adiabatic. The semi-implicit method for pressure-linked equations algorithm is used for pressure–velocity coupling; the second-order upwind scheme is chosen for discrete momentum equations and energy equations; the second-order difference scheme is used for the pressure. The velocity-inlet boundary condition is applied for the inlet and the pressure-outlet boundary condition is applied for the outlet. The four boundary walls of the unit model are set as symmetry boundary conditions. The upstream bulk temperature is set as 283.15 K. The temperature of the heated tube wall is set as a constant, 350 K. All equations take the convergent criterions of relative residual of 1×10^{-4} except energy which is taken as 5×10^{-7}.

2.4 Data reduction

Some formulas used in the post-processing are defined as

$$Re = \frac{\rho D_\mathrm{h} V_\mathrm{in}}{\mu}, \tag{2}$$

$$D_\mathrm{h} = \frac{4(P_\mathrm{t}^2 - \pi d_\mathrm{o}^2/4)}{\pi d_\mathrm{o}}, \tag{3}$$

$$\Delta T = \frac{T_\mathrm{in} - T_\mathrm{out}}{\ln\left(\dfrac{T_\mathrm{in} - T_\mathrm{w}}{T_\mathrm{out} - T_\mathrm{w}}\right)}, \tag{4}$$

$$h = \frac{c_\mathrm{p}\rho V_\mathrm{in} A_\mathrm{in}(T_\mathrm{in} - T_\mathrm{out})}{A_\mathrm{o}\Delta T}, \tag{5}$$

$$Nu = \frac{hD_\mathrm{h}}{\lambda}, \tag{6}$$

$$\Delta p = p_\mathrm{in} - p_\mathrm{out}, \tag{7}$$

$$f = \frac{D_\mathrm{h}}{L}\left(\frac{2\Delta p}{\rho V_\mathrm{in}^2}\right), \tag{8}$$

where Re is the Reynolds number; V_in stands for the mean velocity for the shell side at the cross-section where there are no baffles; D_h represents the hydraulic diameter; A_in is the flow cross-section area of the unit duct; ΔT is the log-mean temperature difference; T_w is the temperature of the tube wall; T_in and T_out are the inlet and outlet temperatures of the working fluid at the shell side, respectively; c_p is the specific heat capacity; A_o is the outer heat transfer area of tubes; Nu is the mean Nusselt number; h is the averaged convection heat transfer coefficient of the tube walls; Δp is the pressure drop; p_in and p_out are the inlet and outlet pressures of the working fluid at the shell side, respectively; f represents the average friction factor; L is the unit duct length along the flow direction.

2.5 Code validation and grid independence

In order to verify the solution independency of the grid, the grid-dependency is checked for three different grids for the HCBetsw-STHX. The geometric parameters of the HCBetsw-STHX for the grid-independency test are listed in Table 1. The grids checked have 2.4, 4.0, and 4.9 million cells, respectively. The obtained Nu and f of the three grid systems are shown in Fig. 8. As shown in Fig. 8, the error between the finest grid having 4.9 million cells and the grid having 2.4 million cells is less than 3% for the heat transfer coefficient and less than 1% for the friction coefficient. Therefore, the settings of the grid of the medium system are used for further investigations in the current study. Similarly, the grid independence test is also carried out for the RRB-STHX.

For the HCBetsw-STHX, there are no experimental results in the open literature. To validate the reliability of the numerical model, non-staggered tubes supported by RRB are computed and compared with the results obtained by Dong et al. (2008). The geometric parameters of the model for model validation are listed in Table 2. The computed Nu numbers are plotted in Fig. 9. It can be seen from Fig. 9 that the relative maximum deviation is within 7%. Such a good agreement shows the reliability of the present physical model and numerical method.

Table 1 Geometric parameters of the HCBetsw-STHX for grid-independency test (unit: mm)

d_o	P_t	L_b	a	b	c	t_b	P_c	d_c	l_{et}
25	32	400	10	10	10	3	40	14	4

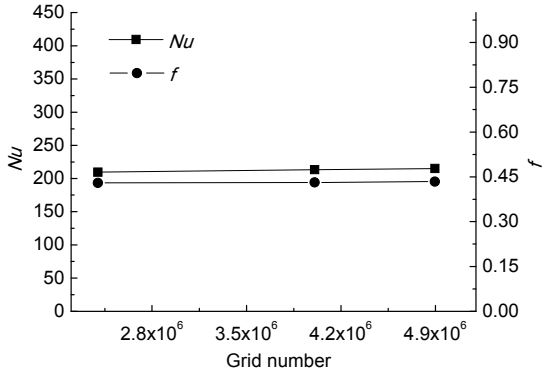

Fig. 8 Mesh independency results of the HCBetsw-STHX

Table 2 Geometric parameters of the RRB-STHX for model validation (unit: mm)

d_o	P_t	d_R*	L_b
25	32	6	400

* d_R is the diameter of round rod baffle

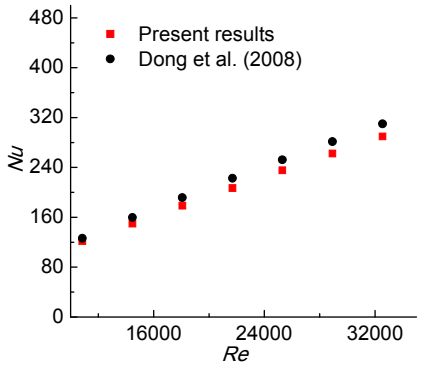

Fig. 9 Model validation of numerical code of RRB- STHX

3 Theory of the Taguchi method

The Taguchi method combines system design, parameter design, and tolerance design procedures to achieve a robust process for the best product quality. In this study, the parameter design based on CFD is used. The general optimization process of parameter design by the Taguchi method is listed below:

1. Choose the optimization objective;
2. Specify the control factors and their levels;
3. Do CFD numerical tests by orthogonal array;
4. Make a signal-noise ratio (SNR) analysis;
5. Show the effect of control factors by main effect plots;
6. Find the optimal levels for the control factors;
7. Perform confirmation tests;
8. Validate the optimization results.

It is worth noting that the Taguchi method used in this study is similar to that described in (Wang et al., 2016) where more details can be found.

3.1 Selection of optimization objectives

For STHX, Nu and f are often used to depict the heat transfer and flow friction characteristics, respectively. It is meaningful to know the influence of design factors on them when optimizing. It is well recognized that f usually increases with increasing Nu. In order to evaluate the overall thermal-hydraulic performance of the HCBetsw-STHX, the PEC is used to evaluate the comprehensive performance. It is expressed as follows:

$$\mathrm{PEC}=\frac{Nu_H / Nu_R}{(f_H / f_R)^{1/3}}, \tag{9}$$

where Nu_H and f_H represent Nu and f of the HCBetsw-STHX, respectively, and Nu_R and f_R represent the Nu and f of the reference RRB-STHX, respectively. For the reference RRB-STHX, its geometric parameters are the same as those listed in Table 2 except that the baffle distance is the same as that in the HCBetsw-STHX.

According to the above analysis, Nu_H, f_H, and PEC are selected as the objectives in this study.

3.2 Factors and levels

In the Taguchi method, the factors can be classified into two groups: control and noise factors.

In this numerical simulation of the HCBetsw-STHX, the physical model and the ideal boundary conditions minimize or eliminate the deviation resulting from the noise factors and so those factors are not considered.

Five geometric parameters are selected as the control factors. Three levels of each factor are chosen as shown in Table 3. The other parameters such as the outer tube diameter and the tube pitch are fixed to

25 mm and 32 mm, respectively. The geometric parameters of the profile of the HCB are listed in Table 1.

Table 3 Levels of each factor

Level	A	B	C	D	E
	L_b (mm)	b (mm)	P_c (mm)	d_c (mm)	l_{et} (mm)
1	300	10	20	13	2
2	350	20	30	14	3
3	400	30	40	15	4

3.3 Orthogonal array

In the Taguchi method, orthogonal arrays are used to define the number and sequence of experiments with different combinations of factors and levels. An orthogonal array of L18 (3^5) is established. Detailed information on the orthogonal array is in Table 4. Note that the inlet velocity for all the 18 numerical cases is set to be 0.696 m/s with corresponding *Re* being 14465. It is worth mentioning that the results obtained can be regarded as reliable and independent of the choice of the orthogonal array only if the confirmation test has passed. The detailed procedures of the confirmation test are illustrated in Section 4.3.3.

Table 4 Orthogonal array of L18 (3^5)

Case No.	Control factor				
	A	B	C	D	E
1	1	1	1	1	1
2	1	2	2	2	2
3	1	3	3	3	3
4	2	1	1	2	2
5	2	2	2	3	3
6	2	3	3	1	1
7	3	1	2	1	3
8	3	2	3	2	1
9	3	3	1	3	2
10	1	1	3	3	2
11	1	2	1	1	3
12	1	3	2	2	1
13	2	1	2	3	1
14	2	2	3	1	2
15	2	3	1	2	3
16	3	1	3	2	3
17	3	2	1	3	1
18	3	3	2	1	2

3.4 SNR analysis

The SNR is an important evaluation index of the robustness of product design, and can help an engineer realize the optimal purpose by identifying the best-level combination.

For the optimization of the HCBetsw-STHX, it is well recognized that Nu_H and PEC are expected to be as large as possible while f_H is expected to be as small as possible. So "the larger, the better" criterion is used for the SNR analysis of Nu_H and PEC (Eq. (10)), while "the smaller, the better" criterion is used for the SNR analysis of f_H (Eq. (11)).

$$\mathrm{SNR}_L = -10\log\left(\frac{1}{n}\sum_{i=1}^{n}\frac{1}{Y_i^2}\right), \tag{10}$$

$$\mathrm{SNR}_S = -10\log\left(\frac{1}{n}\sum_{i=1}^{n}Y_i^2\right), \tag{11}$$

where SNR_L and SNR_S represent the performance criterion "the larger, the better" and "the smaller, the better" for the objectives, respectively; Y is the optimization objective calculated from the CFD simulation (i.e. Nu_H, f_H, and PEC in this study); n is the repeated times of each CFD simulation which is taken to be one in this study. It is worth noting that the largest SNR is always expected whether the criterion is "the larger, the better" or "the smaller, the better".

4 Results and discussion

According to the formulas mentioned above, the SNRs for the Nu_H, f_H, and PEC of the HCBetsw-STHX are listed in Table 5.

In the Taguchi method, intuitive analysis is usually used to identify the significance and contribution ratio of every control factor on the optimization object. In intuitive analysis, the ranks of R and contribution ratio values are two indices for describing the effectiveness of control factors. R is the change of three level average SNRs for each factor and is defined in Eq. (12). The contribution ratio is defined in Eq. (13).

$$R = \mathrm{SNR}_{\max,j} - \mathrm{SNR}_{\min,j}, \tag{12}$$

$$\mathrm{Con}(j)=\frac{\mathrm{SNR}_{\max,j}-\mathrm{SNR}_{\min,j}}{\sum_{j=1}^{m}(\mathrm{SNR}_{\max,j}-\mathrm{SNR}_{\min,j})}, \quad (13)$$

where j is the control factor; m represents the total number of control factors.

4.1 Field analysis

The field distribution contours of the sliced plane *XZ* of the whole flow unit duct of RRB-STHX, HCB-STHX, and HCBetsw-STHX are shown in Fig. 10 when the inlet *Re* is 14465, baffle distance is 300 mm, baffle width is 20 mm, coil pitch is 20 mm, coil diameter is 13 mm, and side length of the equilateral triangle is 4 mm. Corresponding comparisons of the outlet temperature, pressure drop, and maximum *Z* velocity of the whole flow unit duct of the RRB-STHX, HCB-STHX, and HCBetsw-STHX are shown in Fig. 11. Furthermore, as turbulence kinetic energy (TKE) is one of the most important criteria reflecting the heat transfer and resistance characteristics, the TKE distribution comparison is also shown in Figs. 10 and 11.

It can be seen from Figs. 10 and 11 that, for RRB-STHX, when fluid passes the rod, due to the decrease of flow area, the high velocity fluid rushes into the space between adjacent tubes; for HCB-STHX, as the blocked flow area is larger than that of RRB-STHX, the maximum *Z* velocity, the pressure drop, the maximum TKE, and the temperature rise of shell side fluid of HCB-STHX are larger than those of RRB-STHX. Thus, the heat transfer enhancement of HCB-STHX is also greater than that of RRB-STHX; for HCBetsw-STHX, the maximum *Z* velocity, the pressure drop, the maximum TKE, and the temperature rise of shell side fluid are larger than those of HCB-STHX. This is mainly because the equilateral triangular cross-sectioned coiled wire induces the secondary circulations, modifies the flow pattern, generates the vortices, and increases the turbulence.

4.2 Factor analysis of Nu_H and f_H

Based on the 18 cases in Table 5 and the calculating formulas mentioned above, factorial effects on SNR-Nu_H, SNR-f_H, and SNR-PEC are obtained as

Table 5 Raw data and corresponding SNRs for each case

Case No.	Nu_H	SNR-Nu_H	f_H	SNR-f_H	Nu_H/Nu_R	f_H/f_R	PEC	SNR-PEC
1	213.02	46.569	0.621	4.132	1.361	6.900	0.715	−2.916
2	213.29	46.579	0.558	5.066	1.363	6.196	0.742	−2.593
3	220.26	46.859	0.560	5.035	1.407	6.219	0.765	−2.324
4	229.27	47.207	0.688	3.254	1.504	8.551	0.736	−2.668
5	233.07	47.350	0.635	3.950	1.529	7.892	0.768	−2.293
6	191.57	45.646	0.360	8.877	1.257	4.475	0.763	−2.354
7	219.25	46.819	0.518	5.719	1.466	7.044	0.765	−2.330
8	190.88	45.615	0.333	9.551	1.276	4.531	0.771	−2.257
9	230.71	47.261	0.688	3.242	1.542	9.368	0.732	−2.714
10	211.15	46.492	0.474	6.483	1.349	5.264	0.775	−2.209
11	245.74	47.810	0.917	0.751	1.570	10.184	0.724	−2.802
12	199.97	46.019	0.475	6.470	1.278	5.272	0.734	−2.686
13	199.67	46.006	0.414	7.658	1.310	5.150	0.759	−2.400
14	201.76	46.097	0.402	7.909	1.324	5.003	0.774	−2.226
15	252.26	48.037	0.914	0.785	1.655	11.362	0.736	−2.661
16	213.35	46.582	0.431	7.308	1.426	5.866	0.791	−2.038
17	207.07	46.322	0.510	5.851	1.384	6.938	0.726	−2.783
18	206.02	46.278	0.456	6.829	1.377	6.199	0.750	−2.501

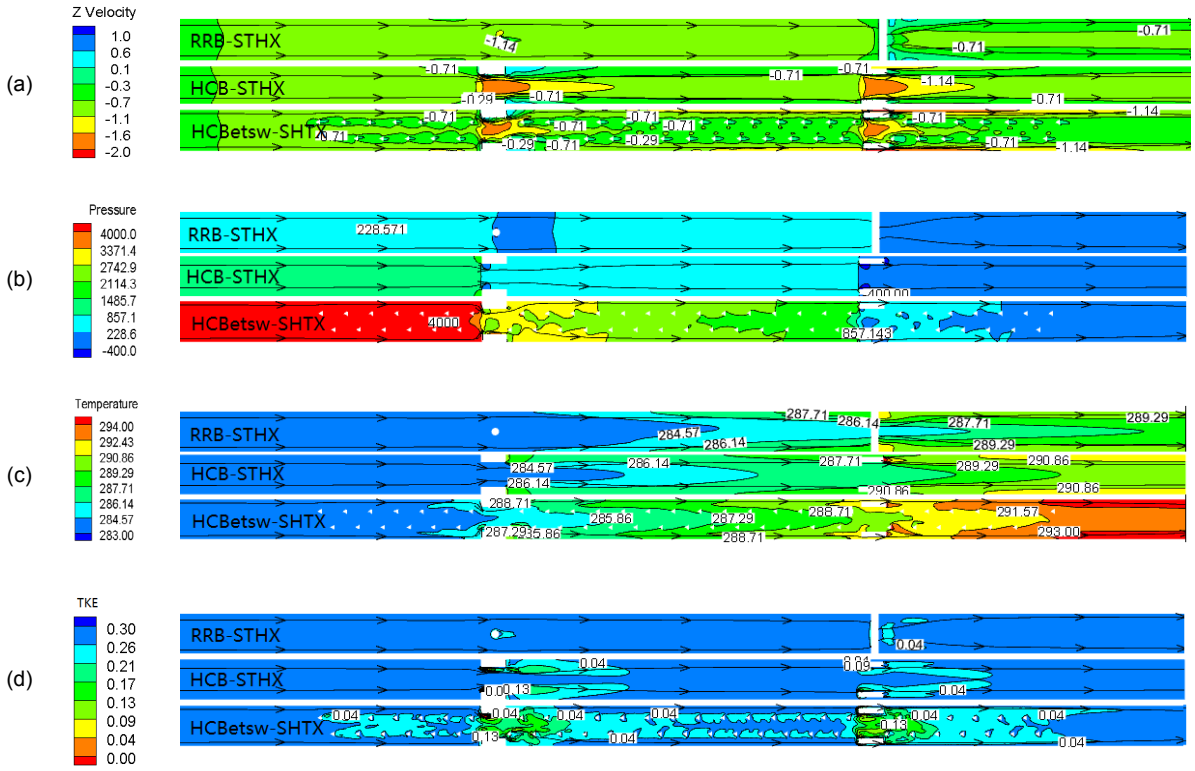

Fig. 10 *Z* velocity (m/s) (a), pressure (Pa) (b), temperature (K) (c), and TKE (m^2/s^2) (d) contours of the sliced plane *XZ* of different flow units when inlet *Re*=14465

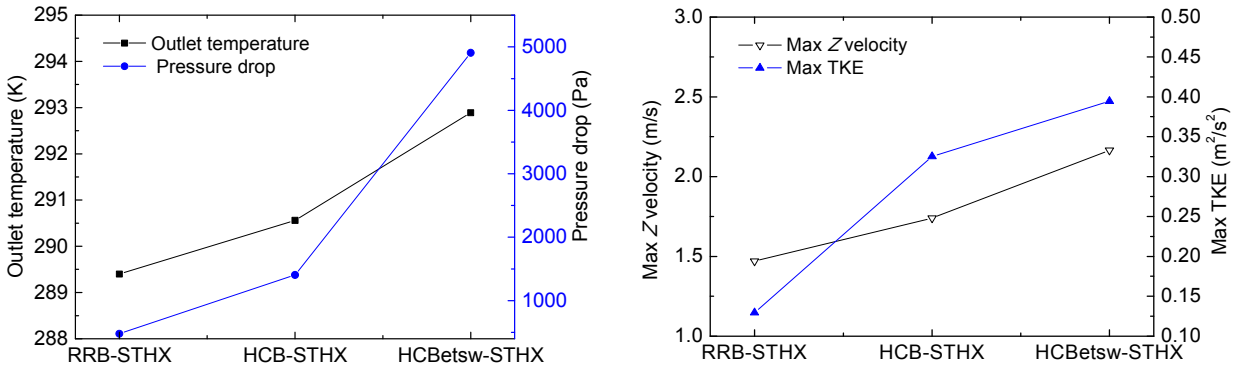

Fig. 11 Comparisons of the outlet temperature and pressure drop (a), and max *Z* velocity and max TKE (b) for the RRB-STHX, HCB-STHX, and HCBetsw-STHX when inlet *Re*=14465

shown in Table 6. The main effect plots are drawn to illustrate the effects of control factors according to the calculated average SNRs of each factor. The main effect plot and the contribution ratio of each factor plot for SNR-Nu_H are shown in Figs. 12 and 13, respectively. The main effect plot and the contribution ratio of each factor plot for SNR-f_H are shown in Figs. 14 and 15 (p.686), respectively.

From Fig. 13, it can be seen that the order of the factor effectiveness for the Nu_H is E>C>A>D>B. The side length of the equilateral triangle (E) has a dominant influence on the Nu_H with a contribution ratio of 45.05%. Next, the coil pitch (C) contributes 36.61%. The sum of contribution ratios of these two factors is more than 81.66%. In contrast, the factor effectiveness of the baffle distance (A), coil diameter (D), and

Table 6 Factorial effect and contribution ratio for the SNR-Nu_H, SNR-f_H, and SNR-PEC

Factor	SNR-Nu_H (dB)			R	Contribution ratio	Rank
	Level 1	Level 2	Level 3			
A	46.721	46.724	46.480	0.244	9.07%	3
B	46.612	46.629	46.684	0.072	2.64%	5
C	47.201	46.509	46.215	0.986	36.61%	2
D	46.536	46.673	46.715	0.179	6.63%	4
E	46.030	46.652	47.243	1.213	45.05%	1
Total				2.693	100%	

Factor	SNR-f_H (dB)			R	Contribution ratio	Rank
	Level 1	Level 2	Level 3			
A	4.660	5.410	6.417	1.760	17.03%	3
B	5.759	5.513	5.206	0.553	5.35%	4
C	3.002	5.949	7.527	4.525	43.78%	1
D	5.703	5.406	5.370	0.333	3.22%	5
E	7.090	5.464	3.925	3.165	30.62%	2
Total				10.336	100%	

Factor	SNR-PEC (dB)			R	Contribution ratio	Rank
	Level 1	Level 2	Level 3			
A	−2.590	−2.430	−2.437	0.155	15.23%	3
B	−2.427	−2.492	−2.540	0.113	11.13%	4
C	−2.757	−2.467	−2.234	0.523	51.44%	1
D	−2.521	−2.484	−2.454	0.068	6.66%	5
E	−2.566	−2.485	−2.408	0.158	15.54%	2
Total				1.016	100%	

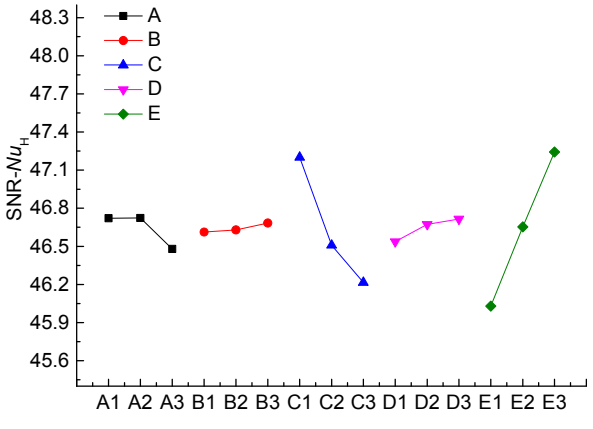

Fig. 12 Main effect plot for the SNR-Nu_H

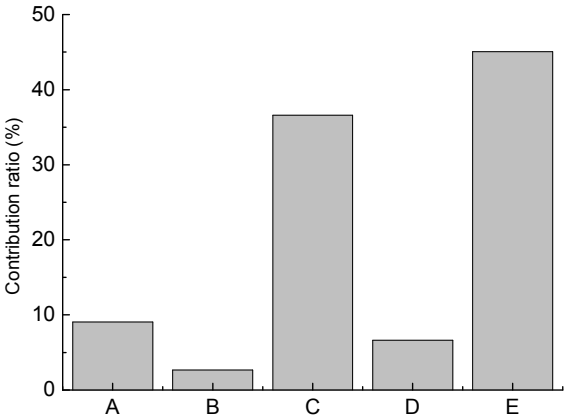

Fig. 13 Contribution ratio of each factor for the SNR-Nu_H

baffle width (B) for the Nu_H is only 9.07%, 6.63%, and 6.19%. This means that the side length of equilateral triangle and coil pitch should be considered first when optimizing the heat transfer characteristics.

To make a further discussion on the effect of each parameter on the Nu_H separately, from Fig. 12, we can see that, for factor A (baffle distance), the Nusselt number first increases and then decreases

with the increase of the baffle distance. The reason is that the heat transfer capacity of the HCBetsw-STHX is affected in two main ways. The first aspect is the mixing effect of the coiled wire on the fluid. The second aspect is the accelerating effect of HCB on the fluid. When the fluid crosses over the HCB, the velocity of the fluid increases rapidly. As a result, the thickness of the liquid boundary layer on the tube wall is reduced. However, as the baffle distance increases, the speed of the fluid will slow down at a certain distance from the HCB, which makes the liquid boundary layer on the tube become thicker again. It can be found that the positive effect of coiled wire and the negative effect of the increase of the baffle distance on the Nusselt number reach a balance for a baffle distance of 350 mm. For factor B (baffle width), the Nusselt number increases with the increase of baffle width. The reason is that with the increase of baffle width, the scope of the zone with the smallest flow area is also extended. Thus, the heat transfer enhancement and the pressure drop are increased. For factor C (coil pitch), the Nusselt number tends to increase with the decrease of the coil pitch. This is mainly because the turbulence intensity and flow path become greater and longer for small coil pitch ratios. This result agrees with that presented by Gunes et al. (2011). For factor D (coil diameter), the Nusselt number increases with the increase of the coil diameter. The reason is that the flow direction is changed by the wire coil; the turbulence intensity and the flow boundary layer thickness become greater and thinner, respectively, with the increase of the coil diameter. For factor E (the side length of equilateral triangle), the Nusselt number increases with the increase in side length. The reason is that the thicker coil wire provides better fluid mixing in the flow field, causing an increase in turbulence intensity, and as a result yields a higher heat transfer rate. From Fig. 12, we can also find that parameters C and E have the largest variation compared with parameters A, B, and D. This further demonstrates that the *Nu* of HCBetsw-STHX is sensitive to the side length of equilateral triangle and the coil pitch.

According to the "the larger, the better" criterion for the Nusselt number, it can be seen from Fig. 12 that the optimum values of the factors for maximum heat transfer are A2B3C1D3E3.

It can be seen from Fig. 15 that the factor effectiveness for f_H is different from that for Nu_H. The coil pitch (C) has the strongest influence on SNR-f_H with a contribution ratio of 43.78%. The side length of the equilateral triangle (E) has the second strongest influence on SNR-f_H with a contribution ratio of 30.62%. The baffle distance (A) and baffle width (B) have contribution ratios of 17.03% and 5.35%, respectively. It is worth noting that the contribution ratio of the coil diameter (D) is only about 3%, which indicates that the effect of the coil diameter is of minor importance on SNR-f_H. According to the above factor effectiveness order of f_H (C>E>A>B>D), the coil pitch and the side length of equilateral triangle should be considered first when optimizing the flow friction characteristics.

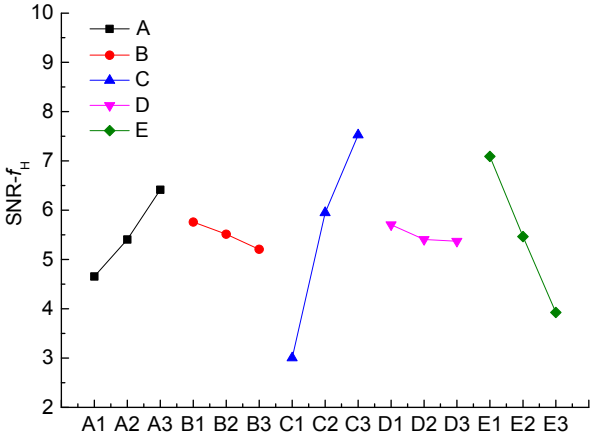

Fig. 14 Main effect plot for the SNR-f_H

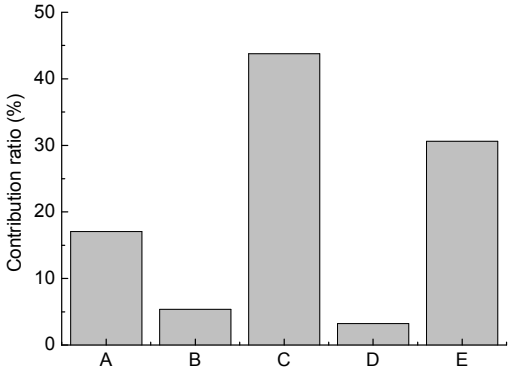

Fig. 15 Contribution ratio of each factor for the SNR-f_H

To consider further the separate effect of each parameter on f_H, it can be seen from Fig. 14 that f_H decreases with the increase of factor A (baffle distance). The reason is that the velocity of jet flow

across the HCB decreases drastically when the baffle distance increases, which causes a significant decrease of flow friction as presented in Fig. 14. For factor B (baffle width), the friction factor decreases with the decrease of baffle width. For factor C (coil pitch), the number of coils is increased by reducing the coil pitch. Therefore, the friction factor increases with the decrease of factor C, due to the fact that increasing the number of coils disturbs the entire flow field and causes more flow friction. The factors D (coil diameter) and E (side length of equilateral triangle) have the same trends. They increase with the increase of the coil diameter and the side length of equilateral triangle, respectively. From Fig.14, we can also find that parameters C and E have the largest variation compared with parameters A, B, and D. This further demonstrates that the friction factor of HCBetsw-STHX is sensitive to the coil pitch and the side length of equilateral triangle.

According to the "the smaller, the better" criterion for f_H, it is clear from Fig. 14 that the optimum values of the factors for minimum flow friction are A3B1C3D1E1.

4.3 Factor optimization of the PEC

It can be seen from Table 5 that Nu_H/Nu_R is in the range of 1.276–1.655; f_H/f_R is in the range of 4.475–11.362; the PEC are all smaller than 0.8. This means that the heat transfer enhancement of HCBetsw-STHX is better than that of RRB-STHX and, simultaneously, the flow friction of the former increases more quickly than that of the latter. As a result, the overall thermal-hydraulic performance of the former is worse than that of the latter.

Factorial effects on SNR-PEC are obtained as shown in Table 6. The main effect plot and contribution ratio of each factor plot for SNR-PEC are shown in Figs. 16 and 17, respectively.

4.3.1 Intuitive analysis

From Fig. 17, the order of the factor effectiveness for the PEC is C>E>A>B>D, which is different from that for Nu_H. From a quantitative perspective, the contribution ratio of every factor is as follows: 15.23% for the baffle distance (A), 11.13% for the baffle width (B), 51.44% for the coil pitch (C), 6.66% for the coil diameter (D), and 15.54% for the side length of the equilateral triangle (E). It shows that the three factors (C, E, and A) have a great influence on the PEC while the coil diameter (D) has a trivial effect on it. This result further illustrates the decisive role of the coil pitch on the overall thermal-hydraulic performance.

According to the "the larger, the better" criterion for the PEC, it is clear from Fig. 16 that the optimum values of the factors for the maximum PEC are A2B1C3D3E3.

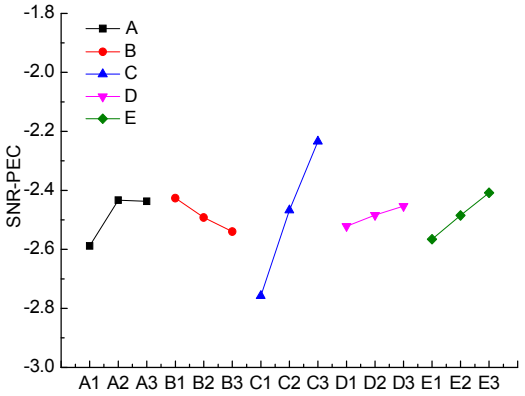

Fig. 16 Main effect plot for SNR-PEC

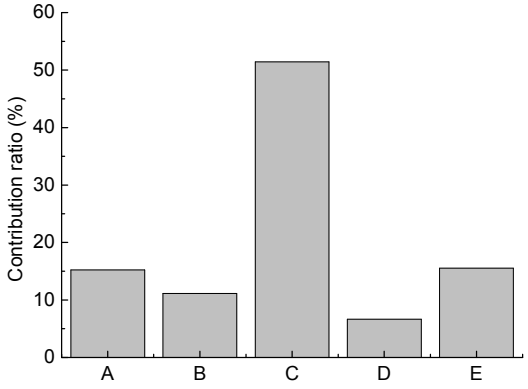

Fig. 17 Contribution ratio of each factor for SNR-PEC

4.3.2 Analysis of variance

The relative significance of the factors in the PEC can be obtained through an analysis of variance (ANOVA). ANOVA is routinely used to provide a measure of confidence. Variance of a factor represents the response of the object to the corresponding factor. The factor which has a larger variance means that it has a more significant effectiveness. The results of ANOVA of HCBetsw-STHX are listed in Table 7. In

the table, DF means the degree of freedom which is obtained from the levels of each factor minus 1 in the orthogonal array; SS means the sum of squares; MS is the mean sum of squares which is obtained from SS divided by DF. *F*-test is the value calculated by the MS of factor divided by the MS of error. $F_{0.05}$ is the statistical probability which is carried out at the 95% confidence level. The calculated $F_{0.05}$ values are compared with the *F*-test to determine which factor has a significant effect on the PEC. If the calculated $F_{0.05}$ value for a factor is larger than that of the *F*-test, this factor can be regarded as significant.

It can be seen from Table 7 that the order of factorial effectiveness is the same as that obtained from the above intuitive analysis; the coil pitch (C) contributes the most, 78.69%. The baffle width (B) and the coil diameter (D) have insignificant effects, 3.7% and 1.32%, respectively. This means that the parameter C (coil pitch) must be considered first during design and optimization. ANOVA also further validates the intuitive analysis.

4.3.3 Reproducibility by confirmation tests

The optimal level combination for the PEC is obtained from the above intuitive analysis. However, this is based on the assumption that there exists additivity of different factors. This assumption requires that the interaction effects among factors are not significant. To confirm the reproducibility of the obtained results, confirmation tests are performed. Two methods are used:

1. Judging the difference between the presumed SN ratio of the optimal combination and that of the optimal case in the orthogonal array.

2. Comparing the PEC of the optimal combination with that of the optimal case in the orthogonal array directly.

The first method is calculated as follows:

$$\mathrm{SNR_p}=\mathrm{SNR_A}+\mathrm{SNR_B}+\mathrm{SNR_C}+\mathrm{SNR_D}+\mathrm{SNR_E}-4\mathrm{SNR_{avg}}=-2.009, \quad (14)$$

where $\mathrm{SNR_p}$ is the presumed SNR-PEC of the optimal combination; $\mathrm{SNR_{avg}}$ is the grand average of SNR-PEC of all 18 cases; $\mathrm{SNR_A}$, $\mathrm{SNR_B}$, $\mathrm{SNR_C}$, $\mathrm{SNR_D}$, and $\mathrm{SNR_E}$ are the optimal level average SNR-PEC of factors A, B, C, D, and E, respectively.

The SNR of the optimal combination taken from Table 5 is −2.038. Thus, it is confirmed that there is reproducibility and that the optimization by the Taguchi method is reasonable.

The second method is calculated as follows:

The PEC of case 16 in Table 5 is taken and compared with that of HCBetsw-STHX with the optimal combination for *Re* between 14465 and 32547 directly. Corresponding results are shown in Fig. 18. Fig. 18 indicates that the optimal combination has higher PEC than case 16 in a wide range of *Re*. The PEC of the optimal combination is improved by 0.19%–1.92% with *Re* ranging from 14465 to 32547. The results further prove that optimization by the Taguchi method is a reasonable one.

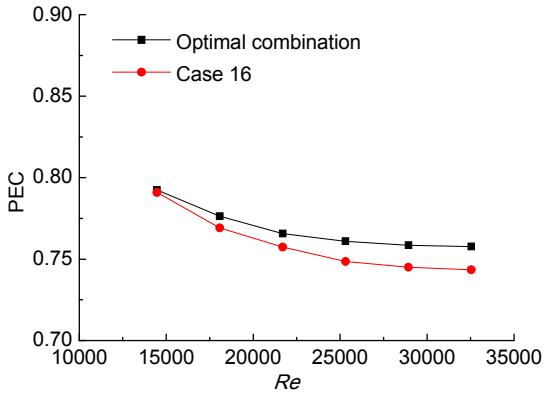

Fig. 18 Variations of PEC with *Re* for HCBetsw-STHX with different factor combinations

Table 7 Analysis of variance for SNR-PEC

Factor	DF	SS	MS	*F*-test	$F_{0.05}$	Contribution ratio
A	2	0.075	0.0374	38.81	4.74	7.16%
B	2	0.039	0.0194	20.07	4.74	3.70%
C	2	0.823	0.4113	426.51	4.74	78.69%
D	2	0.014	0.0069	7.15	4.74	1.32%
E	2	0.094	0.0468	48.51	4.74	8.95%
Error	7	0.0070	0.0010			0.18%
Total	17	1.0503	0.5230			

5 Conclusions

In this study, factor optimization of a parallel-flow STHXs with a new type of anti-vibration hexagon clamping baffle and equilateral triangle cross-sectioned coiled wire is carried out using the Taguchi method. The influences of five geometric parameters on the heat transfer and flow characteristics of the HCBetsw-STHX are numerically analyzed. Some main conclusions are drawn as follows:

1. Over the parameters investigated, the *Nu* of the HCBetsw-STHX is 1.276–1.655 times that of the RRB-STHX, while *f* of the HCBetsw-STHX is 4.475–11.362 times that of the RRB-STHX. Although the PEC of the HCBetsw-STHX is smaller than that of the RRB-STHX, the HCBetsw-STHX can behave better than the RRB-STHX when the flow induced tube vibration is serious or the mass flow of the shell side is small. Furthermore, the HCB is quite suitable for a large and heavy tube bundle as its rigidity is much greater than that of the RRB.

2. The control geometric parameters of the HCBetsw-STHX include baffle distance (A), baffle width (B), coil pitch (C), coil diameter (D), and the side length of the equilateral triangle (E). The results show that the order of the factor effectiveness for *Nu* is E>C>A>D>B, for *f* is C>E>A>B>D, and for the PEC is C>E>A>B>D. The conclusion can be drawn that the coil pitch has a great influence while the baffle width and the coil diameter have little effect. In addition, through intuitive analysis and ANOVA, that conclusion can be further demonstrated.

3. For the PEC of the HCBetsw-STHX, the optimal geometric parameter combination is A2B1C3D3E3. The confirmation tests demonstrate that optimization using the Taguchi method is reasonable. Compared with the best case in the 18 cases, the optimal factor combination improves the PEC by 0.19%–1.92% for *Re* in the range from 14 465 to 32 547.

References

Bas H, Ozceyhan V, 2014. Optimization of parameters for heat transfer and pressure drop in a tube with twisted tape inserts by using Taguchi method. *Arabian Journal for Science and Engineering*, 39(2):1177-1186. https://doi.org/10.1007/s13369-013-0648-4

Bovand M, Rashidi S, Esfahani JA, 2015. Enhancement of heat transfer by nanofluids and orientations of the equilateral triangular obstacle. *Energy Conversion and Management*, 97:212-223. https://doi.org/10.1016/j.enconman.2015.03.042

Chen YP, Sheng YJ, Dong C, et al., 2013. Numerical simulation on flow field in circumferential overlap trisection helical baffle heat exchanger. *Applied Thermal Engineering*, 50(1):1035-1043. https://doi.org/10.1016/j.applthermaleng.2012.07.031

Deng XH, Deng SJ, 1998. Investigation of heat transfer enhancement of roughened tube bundles supported by ring or rod supports. *Heat Transfer Engineering*, 19(2):21-27. https://doi.org/10.1080/01457639808939917

Dong QW, Wang YQ, Liu MS, 2008. Numerical and experimental investigation of shellside characteristics for RODbaffle heat exchanger. *Applied Thermal Engineering*, 28(7):651-660. https://doi.org/10.1016/j.applthermaleng.2007.06.038

El Maakoul A, Laknizi A, Saadeddine S, et al., 2016. Numerical comparison of shell-side performance for shell and tube heat exchangers with trefoil-hole, helical and segmental baffles. *Applied Thermal Engineering*, 109: 175-185. https://doi.org/10.1016/j.applthermaleng.2016.08.067

Gentry CC, 1990. Rodbaffle heat exchanger technology. *Chemical Engineering Progress*, 86(7):48-57.

Gunes S, Manay E, Senyigit E, et al., 2011. A Taguchi approach for optimization of design parameters in a tube with coiled wire inserts. *Applied Thermal Engineering*, 31(14-15):2568-2577. https://doi.org/10.1016/j.applthermaleng.2011.04.022

Huang YQ, Yu XL, Lu GD, 2008. Numerical simulation and optimization design of the EGR cooler in vehicle. *Journal of Zhejiang University-SCIENCE A*, 9(9):1270-1276. https://doi.org/10.1631/jzus.A0820223

Hutagalung FF, 2014. Vibration vulnerability of rod baffle type heat exchanger: case study badak LNG MCR aftercooler. Proceedings of ASME International Mechanical Engineering Congress and Exposition, 13:V013T16A005. https://doi.org/10.1115/imece2014-39673

Keklikcioglu O, Ozceyhan V, 2016. Experimental investigation on heat transfer enhancement of a tube with coiled-wire inserts installed with a separation from the tube wall. *International Communications in Heat and Mass Transfer*, 78:88-94. https://doi.org/10.1016/j.icheatmasstransfer.2016.08.024

Keklikcioglu O, Ozceyhan V, 2017. Entropy generation analysis for a circular tube with equilateral triangle cross sectioned coiled-wire inserts. *Energy*, 139:65-75. https://doi.org/10.1016/j.energy.2017.07.145

Li J, Liu MS, Dong QW, 2005. Numerical investigation of an innovative vibration-proof baffle element for a heat exchanger with longitudinal flows at the shell side. *Journal of Engineering for Thermal Energy and Power*, 20(6): 579-583 (in Chinese). https://doi.org/10.3969/j.issn.1001-2060.2005.06.006

Liu JC, Zhang SY, Zhao XY, et al., 2015. Influence of fin

arrangement on fluid flow and heat transfer in the inlet of a plate-fin heat exchanger. *Journal of Zhejiang University-SCIENCE A* (*Applied Physics & Engineering*), 16(4):279-294. https://doi.org/10.1631/jzus.A1400270

Master BI, Chunangad KS, Pushpanathan V, 2003. Fouling mitigation using helixchanger heat exchangers. Proceedings of the ECI Conference on Heat Exchanger Fouling and Cleaning: Fundamentals and Applications, 1:317-322.

Promvonge P, 2008. Thermal performance in circular tube fitted with coiled square wires. *Energy Conversion and Management*, 49(5):980-987. https://doi.org/10.1016/j.enconman.2007.10.005

Sheng YJ, Chen YP, Cao RB, et al., 2012. Experimental study on shell-side heat transfer and flow resistance performance of heat exchangers with non-round orifice baffles. *Journal of Southeast University* (*Natural Science Edition*), 42(2):318-322. https://doi.org/10.3969/j.issn.1001-0505.2012.02.024

Wang H, Liu YW, Yang P, et al., 2016. Parametric study and optimization of H-type finned tube heat exchangers using Taguchi method. *Applied Thermal Engineering*, 103:128-138. https://doi.org/10.1016/j.applthermaleng.2016.03.033

Wang LK, Sundén B, 2002. Performance comparison of some tube inserts. *International Communications in Heat and Mass Transfer*, 29(1):45-56. https://doi.org/10.1016/s0735-1933(01)00323-2

Wang QW, Chen QY, Chen GD, et al., 2009. Numerical investigation on combined multiple shell-pass shell-and-tube heat exchanger with continuous helical baffles. *International Journal of Heat and Mass Transfer*, 52(5-6):1214-1222. https://doi.org/10.1016/j.ijheatmasstransfer.2008.09.009

Wang YQ, Dong QW, Liu MS, 2007. Characteristics of fluid flow and heat transfer in shellside of heat exchangers with longitudinal flow of shellside fluid with different supporting structures. International Conference on Power Engineering, p.474-479. https://doi.org/10.1007/978-3-540-76694-0_87

Wang YS, Liu ZC, Huang SY, 2011. Experimental investigation of shell-and-tube heat exchanger with a new type of baffles. *Heat and Mass Transfer*, 47(7):833-839. https://doi.org/10.1007/s00231-010-0590-x

Yan LW, Wu JX, Wang ZW, 2004. Industrially experimental investigations and development of the curve-ROD baffle heat exchanger. *Journal of Shanghai University* (*English Edition*), 8(3):337-341. https://doi.org/10.1007/s11741-004-0075-6

Yang J, Liu W, 2015. Numerical investigation on a novel shell-and-tube heat exchanger with plate baffles and experimental validation. *Energy Conversion and Management*, 101:689-696. https://doi.org/10.1016/j.enconman.2015.05.066

You YH, Chen YQ, Xie MQ, et al., 2015. Numerical simulation and performance improvement for a small size shell-and-tube heat exchanger with trefoil-hole baffles. *Applied Thermal Engineering*, 89:220-228. https://doi.org/10.1016/j.applthermaleng.2015.06.012

Yun JY, Lee KS, 2000. Influence of design parameters on the heat transfer and flow friction characteristics of the heat exchanger with slit fins. *International Journal of Heat and Mass Transfer*, 43(14):2529-2539. https://doi.org/10.1016/s0017-9310(99)00342-7

Zeng M, Tang LH, Lin M, et al., 2010. Optimization of heat exchangers with vortex-generator fin by Taguchi method. *Applied Thermal Engineering*, 30(13):1775-1783. https://doi.org/10.1016/j.applthermaleng.2010.04.009

Zhang JF, He YL, Tao WQ, 2009. 3D numerical simulation on shell-and-tube heat exchangers with middle-overlapped helical baffles and continuous baffles-part I: numerical model and results of whole heat exchanger with middle-overlapped helical baffles. *International Journal of Heat and Mass Transfer*, 52(23-24):5371-5380. https://doi.org/10.1016/j.ijheatmasstransfer.2009.07.006

Zhang JF, Guo SL, Li ZZ, et al., 2013. Experimental performance comparison of shell-and-tube oil coolers with overlapped helical baffles and segmental baffles. *Applied Thermal Engineering*, 58(1-2):336-343. https://doi.org/10.1016/j.applthermaleng.2013.04.009

中文概要

题　目： 基于田口方法的带新型防振折流板和线圈的平行流换热器参数优化

目　的： 圆形折流杆管壳式换热器容易发生流体诱发振动，从而引起管束失效。本文旨在探索壳程采用正三角形截面的线圈和六边形防振折流板的平行流换热器的传热特性和传热强化机理。

创新点： 1. 提出一种具有防振功能的带六边形折流板和正三角形截面螺旋线圈的平行流管壳式换热器；2. 采用田口方法揭示几何参数对传热和流动性能的影响；3. 以提高换热器的综合性能为目标函数，得出最优的几何参数组合。

方　法： 1. 采用数值模拟方法和田口方法，分析带六边形防振折流板和正三角形截面线圈的平行流换热器几何参数对传热流动特性的影响；2. 综合对比分析速度、压力、温度和湍流场分布的影响，揭示传热强化机理。

结　论： 1. 得到了不同几何参数对传热和流动的影响程度；其中，线圈的节距对传热和流动的影响程度最大，而六边形夹持防振折流板厚度的影响最小。2. 采用田口方法优化后的结构较原结构的综合性能提高 0.19%~1.92%。

关键词： 优化；平行流；六边形夹持；抗振折流板；圆形线圈；田口方法